

CERN - European Organization for Nuclear Research

LCD-Note-2012-008

Correction of beam-beam effects in luminosity measurement in the forward region at CLIC

S. Lukić*

** Vinča Institute, University of Belgrade, Belgrade, Serbia*

January 21, 2013

Abstract

Procedures for correcting the beam-beam effects in luminosity measurement at CLIC at 3 TeV CM energy are described and tested using Monte Carlo simulations:

- Correction of the angular counting loss due to the combined Beamstrahlung and initial-state radiation (ISR) effects, based on the reconstructed velocity of the collision frame of the Bhabha scattering.
- Deconvolution of the luminosity spectrum distortion due to the ISR emission.
- Correction of the counting bias due to the finite calorimeter energy resolution.

All procedures were tested by simulation. Bhabha events were generated using BHLUMI, and used in Guinea-PIG to simulate the outgoing momenta of Bhabha particles in the bunch collisions at CLIC. Residual uncertainties after correction are listed in a table in the conclusions. The beam-beam related systematic counting uncertainty in the luminosity peak can be reduced to the order of permille.

Presented at: *20th FCAL workshop, Zeuthen, Germany, May 7-9, 2012*

1 Introduction

Luminosity, L , and luminosity spectrum, $\mathcal{L}(E_{CM})$, are key input to analyses of most measurements at a linear collider, including mass and cross-section measurements, as well as the production-threshold scans. Precision measurement of the luminosity is thus essential for the physics programme at a linear collider. The standard way to measure luminosity is to count Bhabha-scattering events recognized by coincident detection of showers in the fiducial volume (FV) in both halves of the luminometer in the very forward region in a given energy range. The number of events N is then divided by the Bhabha cross section σ integrated in the corresponding region of the phase space. This can be formally expressed as follows,

$$L = \frac{N(\Xi(\Omega_{1,2}^{lab}, E_{1,2}^{lab}))}{\sigma(Z(\Omega_{1,2}^{CM}, E_{1,2}^{CM}))}, \quad (1)$$

Here $\Xi(\Omega_{1,2}^{lab}, E_{1,2}^{lab})$ is a function describing the selection criteria for counting the detected events, and $Z(\Omega_{1,2}^{CM}, E_{1,2}^{CM})$ is a function describing the corresponding region of phase space where the cross section is integrated. These functions can be expressed as products $\Xi = \prod_i \xi_i$ and $Z = \prod_i \zeta_i$ where the functions ξ_i and ζ_i are based on specific topological and kinematical properties of the detected/generated pair. For each i , the physical meaning of ξ_i and ζ_i corresponds to each other, although their mathematical form may be different ¹⁾. The set of functions ξ_i and ζ_i includes the angular selection requiring both particles to be detected in the FV, as well as the energy range selection and possible further cuts to eliminate background.

Bhabha scattering is a well known QED process, for which cross-section calculations with relative uncertainty better than 10^{-3} are available [1]. However, at high beam power, the energies and the polar angles of the Bhabha particles are additionally strongly influenced by the beam-beam effects [2, 3]. Because of the random and asymmetric momentum loss when electrons emit Beamstrahlung, the CM frame of the Bhabha process moves with respect to the lab frame with axial velocity different for every colliding pair. As a consequence, Ξ and Z operate on kinematical arguments in different reference frames. Thus, if Ξ and Z have the same form, different regions of the phase space will be covered, leading to a systematic bias in the luminosity measurement. This systematic bias cannot be neglected at the future linear colliders due to the high energy and charge density, and is particularly acute at the 3 TeV CLIC.

A way around this problem is to define Ξ and Z such that the counting rate is independent of the reference frame. Some of the functions ξ_i and ζ_i can be defined invariant to the boost along the beam axis. This is, for example, the case with the cuts on the reconstructed CM energy. However, the requirement that the outgoing particles hit the FV of the detector on both sides does not possess such invariance. In this paper, a definition of ξ_{FV} and ζ_{FV} is proposed such that both the experimental count N and the cross-section σ are reconstructed in the same reference frame, namely the collision frame, which will be properly defined in the appropriate section.

The physical processes affecting the luminosity measurement will be outlined and the used terms and notation defined in Sec. 2. The analysis method with the correction procedures, as well as the test results will be described in Sec. 3. In the conclusions, the main advantages of the presented method are restated, and the final uncertainties are listed and briefly discussed.

¹See in particular Sec. 3.2 and Eqs. 6 and 7

2 The physical processes affecting the luminosity measurement and the outline of the correction procedure

The sequence of physical processes relevant to the present discussion is schematically represented in Fig. 1. Due to the pinch effect during the bunch collision, both particles may emit Beamstrahlung photons and so lose energy and momentum before the interaction. Thus in general, $E_{CM} < E_0 \equiv 2E_{beam}$. The CM energy distribution at this stage is the actual luminosity spectrum $\mathcal{L}(E_{CM})$. The probability of the Bhabha scattering scales with $1/s \equiv 1/E_{CM}^2$, resulting in the CM energy distribution of the Bhabha events $\mathcal{B}(E_{CM}) \propto \mathcal{L}(E_{CM})/E_{CM}^2$. The Bhabha process is itself accompanied by emission of the initial-state radiation (ISR) that is nearly collinear with the initial particle momenta, as well as the final-state radiation (FSR) that is approximately collinear with the outgoing particle momenta. Since the ISR is nearly collinear with the beam axis, it misses the luminometer, so that the CM energy reconstructed from the detected particles is $E_{CM,rec} < E_{CM}$, and the corresponding spectrum is,

$$h(E_{CM,rec}) = \int_0^{E_{max}} \mathcal{B}(E_{CM}) \frac{1}{E_{CM}} \mathcal{I}\left(\frac{E_{CM,rec}}{E_{CM}}\right) dE_{CM} \quad (2)$$

where $\mathcal{I}(x)$ is the distribution of the fractional CM energy losses due to ISR. $\mathcal{I}(x)$ is approximately independent of E_{CM} .

Due to the finite energy resolution of the LumiCal, the reconstructed spectrum is smeared, which can be represented as a convolution with a normalized Gaussian².

$$h^*(E_{CM,rec}) = \frac{1}{\sqrt{2\pi}\sigma} \int_0^{\infty} h(E'_{CM,rec}) \exp\left(-\frac{(E_{CM,rec} - E'_{CM,rec})^2}{2\sigma^2}\right) dE'_{CM,rec} \quad (3)$$

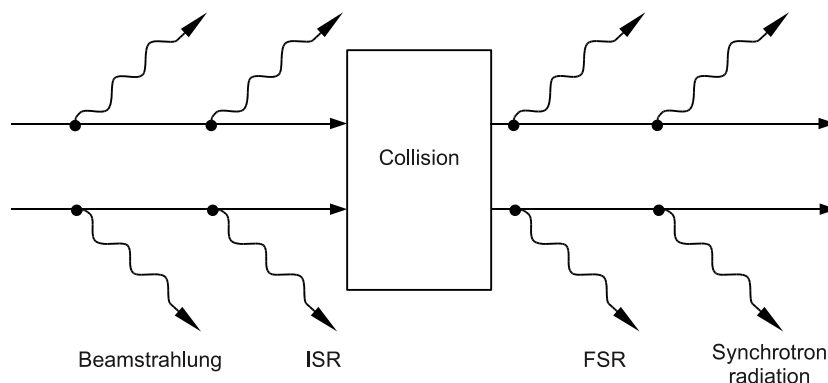


Figure 1: Schematic representation of the physical processes affecting the luminosity measurement

²Strictly speaking, the smearing width depends on the deposited energy of the showers. However, as only a relatively narrow energy range is being analyzed here, the smearing width will be treated as being approximately constant.

The term *collision frame* will be used here for the frame of the two-electron system³⁾ after emission of Beamstrahlung and ISR and before emission of the FSR⁴⁾. The scattering angle in the collision frame is denoted θ^{coll} . Due to the radiation prior to the collision, the collision frame has a non-zero velocity $\vec{\beta}_{coll}$, and the outgoing particle angles in the lab frame, θ_1^{lab} and θ_2^{lab} , are not symmetric. In a significant fraction of the total number of events, the acollinearity is so large that the two particles are not detected in coincidence within the FV of the LumiCal. In this way, Beamstrahlung and ISR induce an *angular counting loss* of Bhabha events.

Finally the electromagnetic deflection (EMD) of the outgoing electrons in the field of the opposing bunch induces a small additional angular counting loss.

The outline of the procedure of the Bhabha-count analysis is as follows:

1. Reconstruct the CM energy $E_{CM,rec}$ and the collision-frame velocity β_{coll} for each pair detected in the FV of the LumiCal, from the angles and the measured particle energies.
2. Assign weight to events to correct for reduced acceptance due to $\vec{\beta}_{coll}$, as shown in Sec. 3.2.
3. Deconvolution of the ISR energy loss $\mathcal{I}(x)$ from the spectrum $h^*(E_{CM,rec})$, in order to restore the $\mathcal{B}^*(E_{CM})$ CM energy spectrum of the Bhabha events (see Sec. 3.3).
4. Integrate $\mathcal{B}^*(E_{CM})$ in the energy range of measurement.
5. Correct the systematic effect of the finite energy resolution of the LumiCal on the number of counts in the peak (Sec. 3.4).

The absolute luminosity in the measured energy range is then given by Eq. 1, and the approximate differential form of the luminosity spectrum with the LumiCal energy smearing can be obtained as $\mathcal{L}^*(E_{CM}) = \mathcal{B}^*(E_{CM})E_{CM}^2$.

3 Analysis and correction procedures

3.1 Simulation methods used to test the analysis procedure

To test the analysis procedure, Bhabha events in the bunch-collision were simulated with the Guinea-PIG software [3]. The initial bunch coordinate- and momentum distributions were taken from the simulation results by D. Schulte et al. [4]. The coordinate distribution covered more than 10σ bunch widths both in the horizontal and the vertical directions. The angular distribution of the particles in the bunch was quasi-Gaussian, with transverse emittance of 660 nm rad in the horizontal, and 20 nm rad in the vertical direction. The bunch collision was simulated in the CM frame of the colliding bunches, which is equivalent to a head-on collision with zero crossing angle. The beam overlap reduction due to the crossing angle is offset by the crab-crossing scheme.

³Unless stated otherwise, electron always refers to electron or positron

⁴In reality, ISR and FSR can not be cleanly separated even theoretically, due to the quantum interference between them. Thus in practice, the collision frame is defined as the CM frame of the final electrons together with all radiation within a given tolerance angle with respect to the final electron momenta. The assumption of clean separation between ISR and FSR introduces a small uncertainty in the final result.

The Bhabha events were produced using a method resembling that by C. Rimbault et al. [5]: After generating the initial four-momenta of the colliding e^-e^+ pairs, the decision is made by Guinea-PIG whether the Bhabha scattering will be realized in the collision, based on the $1/s$ proportionality of the Bhabha cross section. If a Bhabha event is to be realized, the final four-momenta are picked from a file generated at 3 TeV by the BHLUMI generator [6]. The momenta are then scaled to the CM energy of the colliding pair, rotated to match the collision axis, and then boosted back to the lab frame. Finally the outgoing Bhabha electrons are tracked to simulate the electromagnetic deflection. Nearly four million Bhabha events were generated in the polar angle region between 10 and 200 mrad in the generator frame, with additional cuts between 37 and 90 mrad in the collision frame.

The interaction with the detector was approximated in the following way:

- The four-momenta of all electrons and photons within 5 mrad of the most energetic shower were summed together on each side. The 5 mrad criterion corresponds closely to the Molière radius of the high-energy showers in the LumiCal [7]. The Beamstrahlung photons were not included as they are emitted close to the beam axis. For synchrotron radiation, the characteristic emission angles are of the order $1/\gamma$, which is smaller than 10^{-3} mrad for electron energies in the TeV range, therefore photon and electron four-vectors can be added.
- The energy resolution of the LumiCal was included by adding random fluctuations to the final particle energies. The random fluctuations were sampled from the Gaussian distribution with an energy-dependent standard deviation $\sigma_E = a\sqrt{E}$, with $a = 0.21$ [8, 9].
- The finite angular resolution of the LumiCal was included by adding random fluctuations to the final particle polar angles. The nominal value of $\sigma_\theta = 2.2 \times 10^{-5}$ estimated for the ILC version of LumiCal [7] was used. Higher values for σ_θ were also tested.

The FV of the LumiCal at CLIC corresponds to the angular range between 43 and 80 mrad around the respective beam axes.

3.2 Invariant counting in the collision frame

The movement of the collision frame with respect to the lab frame is responsible for the acollinearity leading to the angular counting loss. The velocity of the collision frame with respect to the lab frame $\vec{\beta}_{coll}$, can be approximately calculated from the measured polar angles. If $\vec{\beta}_{coll}$ is taken to be collinear with the z -axis, the expressions for the boost of the Bhabha scattering angles into the lab frame give,

$$\beta_{coll} = \frac{\sin(\theta_1^{lab} + \theta_2^{lab})}{\sin \theta_1^{lab} + \sin \theta_2^{lab}} \quad (4)$$

Eq. 4 does not depend on any assumptions about the number of emitted ISR and Beamstrahlung photons, nor on their direction, apart from the assumption that the vector sum of their

momenta is collinear with the z-axis⁵).

If events from a subset characterized by a given β_{coll} are plotted in the $|\tan \theta_2|$ vs. $|\tan \theta_1|$ graph, they lie on a curve displaced from the central diagonal, as schematically represented by the dashed line in Fig. 2. As can be seen from the figure, the range of accepted scattering angles decreases with increasing β_{coll} . The effective limiting angles θ_{min}^{coll} and θ_{max}^{coll} for the subset of events characterized by a given β_{coll} are obtained by boosting θ_{min} and θ_{max} into the collision frame.

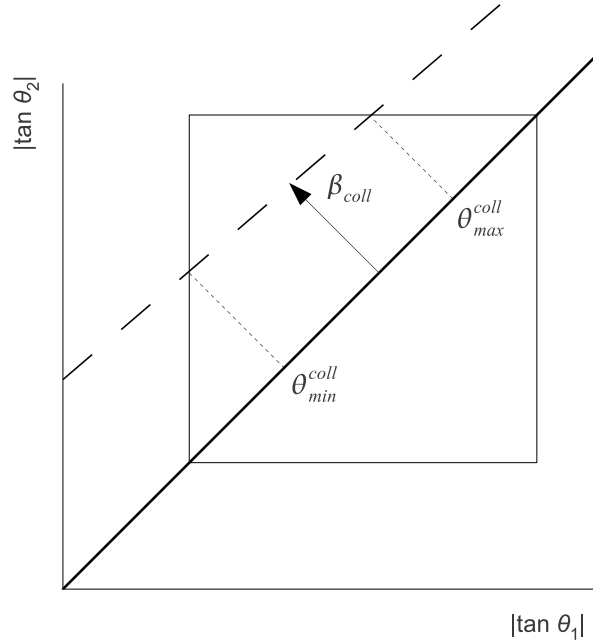


Figure 2: Schematic representation of the distortion of the polar angles due to the movement of the collision frame. The box represents the region in which both electrons hit the FV, and the dashed line represents the event subset characterized by a given β_{coll} . θ_{min}^{coll} and θ_{max}^{coll} denote the effective limiting scattering angles for this subset.

To account for the smaller acceptance of the events characterized by a given β_{coll} , every event has to be weighted with the appropriate correction factor. In this way, the number of events between θ_{min} and θ_{max} in the collision frame is recovered for each β_{coll} subset separately. The weighting factor is defined in the following way:

⁵ Strictly speaking, $\vec{\beta}_{coll}$ has a small radial component β_ρ , which is larger than 0.01 in only about 5 permille of cases. However, the influence of β_ρ on the polar angles of the Bhabha pair is almost indistinguishable from an additional axial boost. Thus for the purpose of recovering the counting loss due to the acollinearity, β_{coll} is approximately treated as a scalar quantity.

$$w(\beta_{coll}) = \frac{\int_{\theta_{\min}}^{\theta_{\max}} \frac{d\sigma}{d\theta} d\theta}{\int_{\theta_{\min}^{coll}}^{\theta_{\max}^{coll}} \frac{d\sigma}{d\theta} d\theta}. \quad (5)$$

The FV selection function is thus defined as⁶⁾,

$$\xi_{FV} = \begin{cases} w & ; \theta_{1,2}^{lab} \in FV \\ 0 & ; otherwise \end{cases} \quad (6)$$

Using this FV selection function, the number of events N satisfying the condition $\theta^{coll} \in (\theta_{\min}, \theta_{\max})$ in the collision frame is reconstructed. The corresponding function ζ_{FV} for the cross-section integration is thus,

$$\zeta_{FV} = \begin{cases} 1 & ; \theta^{coll} \in (\theta_{\min}, \theta_{\max}) \\ 0 & ; otherwise \end{cases} \quad (7)$$

3.2.1 Test of the collision-frame counting method

To test the counting method, histograms of $E_{CM,rec}$ reconstructed from kinematic parameters of the detected particles were generated in the following way:

Control histogram : All events with the scattering angle in the collision frame θ^{coll} such that $\theta_{\min} < \theta^{coll} < \theta_{\max}$ are accepted. Therefore this histogram is not affected by counting losses due to Beamstrahlung and ISR. This is, of course, only possible in the simulation.

Uncorrected histogram : Events hitting the FV of the LumiCal in the lab frame.

Corrected histogram : Events hitting the FV of the LumiCal in the lab frame, stored with the weight w calculated according to Eq. 5

The full kinematical information, including the particle energy, was used for the reconstruction of the CM energy. The four-momenta of collinear photons were added to the electron four-momenta as described in Sec. 3.1. Apart from the collinearity criterion, no distinction was made between the ISR and the FSR photons.

To calculate the correction weight w , the approximate expression for the angular differential cross section $d\sigma/d\theta \approx \theta^{-3}$ was used.

The results are shown in Fig. 3. The control spectrum is plotted in black, red is the spectrum affected by the counting loss, green is the corrected spectrum.

The blue line represents the events inaccessible to the correction due to the high value of β_{coll} . In the subsets of events characterized by β_{coll} above a certain threshold, at least one electron is always lost (see Fig. 2). However, for such events, the Beamstrahlung-ISR energy loss is also

⁶⁾By the standard definition of the polar angle θ , the interval corresponding to the FV on side of the IP is $(\theta_{\min}, \theta_{\max})$, and on the other side of the IP, $(\pi - \theta_{\max}, \pi - \theta_{\min})$

above a certain minimum, so that they are only present in significant number below 2200 GeV. A small number of high- β_{coll} events are also present at energies above 2200 GeV, as seen in the zoomed figure (Fig. 3, right), where these events are scaled by a factor 100. In these events, $\vec{\beta}_{coll}$ has a relatively high radial component, due to the off-axis radiation before collision. This increases the acollinearity of such events relative to other events with similar energy loss (see footnote 5). The relative contribution of these events to the peak integral above 95% of the nominal CM energy is of the order of 2×10^{-5} .

Before correction, the counting loss in the peak integral above 95% of the nominal CM energy was 3.8%. After correction, the residual relative deviation in the peak with respect to the control spectrum is $(-0.1 \pm 0.4(\text{stat.})) \times 10^{-3}$. In the tail between 80% and 90% of the nominal CM energy, the counting loss before correction was 43.1%. After correction, the residual relative deviation in the tail is $(-3.6 \pm 1.8(\text{stat.})) \times 10^{-3}$, which includes a deviation of $(-2.7 \pm 0.1) \times 10^{-3}$ due to the lost events in the tail. The statistical uncertainty of the residual deviation was estimated taking into account the correlations between the corrected and the control spectra. The precision of the Beamstrahlung-ISR correction is of the order of permille despite the presence of the following sources of systematic uncertainty of the correction:

- The assumption that the deformation of the Bhabha angles induced by Beamstrahlung and ISR is well described as a Lorentz boost along the beam axis (this is the source of the "lost" events in the peak),
- The use of the approximate angular differential cross section for the Bhabha scattering in the calculation of w ,
- Assumption that all ISR is lost, and all FSR is detected (this assumption has, in principle, an influence on the calculation of β_{coll} , and consequently of w).

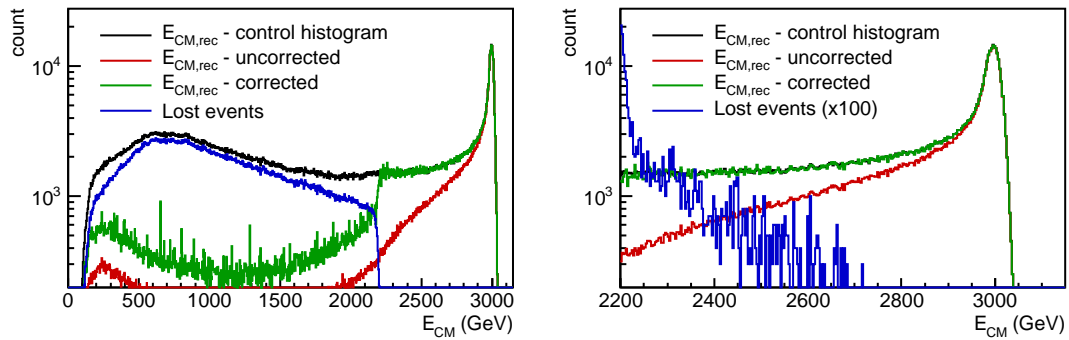


Figure 3: Correction of the counting loss due to Beamstrahlung and ISR. Left: whole spectrum; right: zoom on energies above 2200 GeV. Black: Simulated control spectrum without counting loss due to Beamstrahlung and ISR; red: Reconstructed E_{CM} spectrum affected by the counting loss; green: Reconstructed spectrum with correction for the counting loss due to Beamstrahlung and ISR; blue: events inaccessible to the correction due to high β_{coll} (see text).

Table 1: Dependence of the uncorrected and the corrected peak-count deviations on the polar-angle uncertainty of the LumiCal

$\Delta\theta$ (mrad)	Uncorrected (10^{-3})	Corrected (10^{-3})
0.010	-38.1 ± 0.3	-0.0 ± 0.4
0.022	-38.2 ± 0.3	-0.1 ± 0.4
0.05	-38.3 ± 0.3	-0.1 ± 0.4
0.10	-38.8 ± 0.3	-0.3 ± 0.4
0.20	-40.1 ± 0.4	-0.4 ± 0.4
0.50	-46.8 ± 0.4	-1.6 ± 0.4

A test of this method for the case of ILC at nominal CM energies of 0.5 and 1 TeV, and for a wide range of beam-parameter uncertainties is reported in Ref. [10]. After correction of the lost events, precision of a fraction of permille is achieved in the upper 80% of energy, independently of the precision with which the beam parameters are known.

3.2.2 Effect of the particle energy- and polar-angle resolution on the Beamstrahlung-ISR counting loss

The relative energy resolution of a calorimeter can be parametrized as a quadratic sum of an energy-dependent stochastic term and a constant *shower leakage* term [11].

$$\frac{\sigma_E}{E} = \sqrt{\frac{a^2}{E} + b^2} \quad (8)$$

The 40-layer design of the LumiCal for CLIC is assumed to be well described by the parametrization with the constant term b equal to zero [8]. A conservative limit for the constant term can be taken to be 1.1%, based on the analysis in Ref. [11], made for the ILC version of LumiCal, with only 30 layers (implying considerable leakage at 1.5 TeV). The correction procedure was therefore tested with three different values of the constant term b : 0, 0.35% and 1.1%, while the stochastic term was kept at $a = 0.21$. In all these tests, both the uncorrected Beamstrahlung-ISR counting loss, and the residual deviation after correction agree within their respective statistical uncertainties. Only results for $b = 0$ are presented in this paper.

Tests were also performed with different values of the polar-angle uncertainty of the LumiCal in the range between 0.01 mrad and 0.5 mrad, beside the nominal value of 0.022 mrad [7]. The results of these tests are shown in Tab. 1. One may note that the uncorrected counting loss increases significantly when the polar-angle uncertainty increases above 0.1 mrad. The effect on the count deviation in the corrected peak is, however, about six times smaller.

3.3 Deconvolution of the ISR energy loss

After correcting for the angular counting loss, the ISR energy loss can be deconvoluted from the resulting spectrum $h(E_{CM,rec})$ to restore the CM energy spectrum of the Bhabha events

$\mathcal{B}^*(E_{CM})$ ⁷). When Eq. 2 is binned in N sufficiently narrow bins, it takes approximately the discrete form,

$$h_i \approx \sum_{j=1}^N \mathcal{I}_{ij} \mathcal{B}_j^* \quad (9)$$

Where,

$$\begin{aligned} h_i &= \int_{(i-1)\Delta E}^{i\Delta E} h(E_{CM,rec}) dE_{CM,rec} \\ \mathcal{B}_j^* &= \int_{(j-1)\Delta E}^{j\Delta E} \mathcal{B}^*(E_{CM}) dE_{CM} \\ \mathcal{I}_{ij} &= \int_{\frac{i-1/2}{j}}^{\frac{i-1/2}{j-1}} \mathcal{I}(x) dx \end{aligned} \quad (10)$$

As the \mathcal{I}_{ij} matrix has triangular form, eq. 9 can be solved for \mathcal{B}_j^* exactly, using the Jacobi method. The solution proceeds from high-energy towards the lower-energy bins, introducing an increasing uncertainty towards lower energies.

To obtain $\mathcal{I}_{i,j}$, the function $\mathcal{I}(x)$ was parametrized by the beta distribution used for the parametrization of the beam spectra of linear colliders [12],

$$\mathcal{I}(x) = a_0 \delta(x-1) + \begin{cases} a_1 x^{a_2} (1-x)^{a_3} & ; x < 1 \\ 0 & ; x \geq 1 \end{cases} \quad (11)$$

The parameters were obtained by fitting Eq. 11 to the fractional CM energy distribution after ISR, reconstructed from the same BHLUMI data set as used in Guinea-PIG. The fit was performed with variable binning in order to have sufficiently fine binning near $x = 1$, while avoiding large differences in statistical uncertainties for individual bins. The data histogram was first normalized to the unit integral. The results are shown in Fig. 4. The parameter a_0 was obtained as the ratio of the number of counts in the narrow peak above $x = 0.99995$ to the number of counts in the entire spectrum, and the remaining coefficients were obtained by fitting the function to the data in the range (0.7, 0.99995)^{8) 9)}.

⁷The Bhabha-event spectrum is marked with a star here, because it is smeared by the finite energy resolution of the LumiCal. See Sec. 3.4.

⁸The angular cuts in the lab frame cause significant losses in the distribution for $x < 0.5$ because high energy loss in ISR emission correlates with high acollinearity. This affects the overall normalization, and thus the value of a_0 . The value of a_0 obtained here is appropriate for the deconvolution of the simulated spectrum where the same set of BHWIDE samples was used. However, for the analysis of the real experimental data, the distribution without cuts in the lab frame should be used.

⁹The functional form of Eq. 11 suggests that the ratio a_0/a_1 can be fixed by the normalization requirement. However, the beta distribution fails to properly describe the form of $\mathcal{I}(x)$ for $x < 0.7$ (regardless of the angular cuts

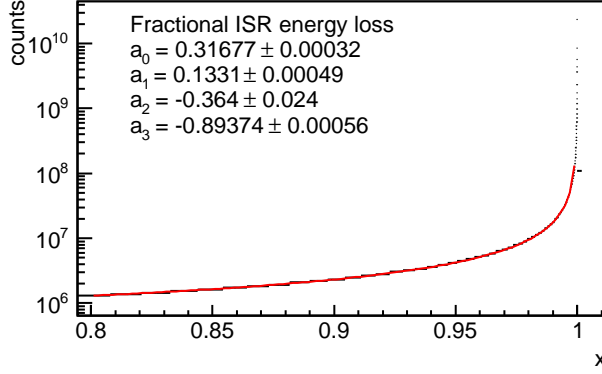


Figure 4: Fit of the relative energy-loss distribution due to the ISR.

From the normalization of the data histogram, it follows that, $a_0 + Ca_1 = 1$, from which the covariance of a_0 and a_1 was calculated as $\text{cov}(a_0, a_1) = \langle (a_0 - \langle a_0 \rangle)(a_1 - \langle a_1 \rangle) \rangle = -(1/C) \langle (a_0 - \langle a_0 \rangle)^2 \rangle = -(1/C) \sigma_0^2 = -a_1 / (1 - a_0) \sigma_0^2$, where σ_0 is the statistical uncertainty of the parameter a_0 . The correlation of a_0 with a_2 and a_3 was assumed to be zero, and the correlation coefficients between the fitted parameters $a_{1,2,3}$ were calculated from the covariance matrix obtained in the fit procedure. The nonzero correlation coefficients are the following: $\rho_{0,1} = -13\%$, $\rho_{1,2} = 83\%$, $\rho_{1,3} = 96\%$, $\rho_{2,3} = 75\%$.

3.3.1 Test of the deconvolution procedure

In this test, the following histograms were generated:

Control histogram was filled with simulated CM energies before ISR emission, and then smeared with a normalized Gaussian with constant width corresponding to the LumiCal energy-resolution at the peak energy.

Histogram with ISR energy loss $h(E_{CM,rec})$ is the same as the control histogram from Sec. 3.2 – filled with energies reconstructed from the final-state kinematics, and with inclusion of the LumiCal energy resolution.

Deconvoluted histogram was obtained by solving the system of linear equations represented by Eq. 9, taking the binned data of the affected histogram as h_j .

For each histogram, event selection was made on the scattering angles in the collision frame, so that the Beamstrahlung-ISR angular counting loss is not present. This was done in order to assess the accuracy of the deconvolution separately from the Beamstrahlung-ISR counting-loss correction. Results are shown in Fig. 5.

Before deconvolution, the relative counting loss in the peak above 95% of the nominal CM energy was 23.4%. After deconvolution, the relative residual deviation of the peak integral with

in the lab frame discussed above), so that the overall norm is different than the integral of the beta distribution extrapolated from the fit. Therefore, a_1 was allowed to vary freely in the fit.

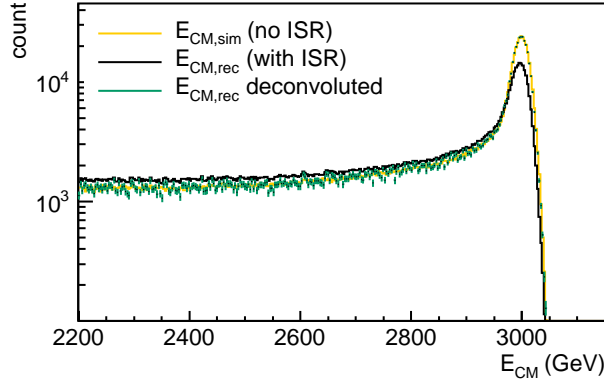


Figure 5: Deconvolution of the ISR deformation of the luminosity spectrum. Yellow: the control histogram – simulated E_{CM} before emission of ISR, smeared with a normalized Gaussian; black: the histogram affected by the ISR energy loss – reconstructed E_{CM} from the detected showers, green: deconvoluted spectrum

respect to the control histograms is $(+1.3 \pm 2.1) \times 10^{-3}$. In the tail between 80% and 90% of the nominal CM energy, the ISR energy loss increases the count by 14.5%. After deconvolution, the remaining deviation in the tail is $(-2.3 \pm 3.9) \times 10^{-3}$.

The contributions from the uncertainties of the fitted parameters of the ISR energy-loss function $\mathcal{I}(x)$ were added to the statistical uncertainty of the residual deviation after deconvolution. The full covariance matrix of the fit parameters was used, together with the partial derivatives of the count estimated by variation of the fit parameters by one sigma, one parameter at a time. With the statistic of about four million generated Bhabha events, the uncertainties due to the fit parameters are $(\delta N/N)_{peak,ISRfit} = 0.53 \times 10^{-3}$ for the peak, and $(\delta N/N)_{tail,ISRfit} = 0.07 \times 10^{-3}$.

When the deconvolution step is tested with a non-zero leakage term in the LumiCal energy resolution, the residual uncertainties agree with the ones presented above within the statistical uncertainties.

3.4 Effect of the LumiCal energy resolution on the counting rate in the peak

The finite energy resolution of the LumiCal introduces a counting bias in two ways:

1. By asymmetric redistribution of events from each side of the sharp energy cut E_{cut} used to define the peak, due to the slope of the underlying distribution at the position of the cut.
2. By cutting off a portion of the low-energy tail of the quasi-Gaussian bell formed by the smearing of the inherent shape of the luminosity peak due to the LumiCal resolution.

The second effect is difficult to precisely correct because of the strong dependence on the position of the energy cut, and because of the uncertainties of the inherent width of the luminosity peak and of the energy resolution, as well as the strong correlations between the fitted

parameters that dominate the spectrum in the peak area (see Eqs. 12 and 13). However, if the energy cut is made at a sufficient distance from the peak, the second effect becomes negligible, and the energy-resolution effect can be precisely corrected based on the parametrization of the functional form of the experimental spectrum after deconvolution of the ISR.

$$\mathcal{B}^*(E_{CM}) = \frac{1}{\sigma\sqrt{2\pi}} \int_0^{\infty} \mathcal{B}(E') \exp\left(-\frac{(E_{CM}-E')^2}{2\sigma^2}\right) dE' \quad (12)$$

If the inherent width of the luminosity peak is neglected, $\mathcal{B}(E_{CM})$ can be parametrized by the beta distribution,

$$\mathcal{B}(E_{CM}) = b_0 \delta(E_{CM} - E_0) + \begin{cases} b_1 E_{CM}^{b_2} (E_0 - E_{CM})^{b_3} & ; E_{CM} < E_0 \\ 0 & ; E_{CM} \geq E_0 \end{cases} \quad (13)$$

One may recall here that the use of a constant standard deviation σ in Eq. 12 is an approximation, as σ depends on the particle energy, and is thus different for different E_{CM} . The systematic error induced by the energy resolution of LumiCal can now be expressed as,

$$\frac{\delta N_{E_{res}}}{N} = \frac{\int_{E_{cut}}^{\infty} \frac{E_{CM}^2}{E_0^2} (\mathcal{B}^*(E_{CM}) - \mathcal{B}(E_{CM})) dE_{CM}}{\int_{E_{cut}}^{\infty} \frac{E_{CM}^2}{E_0^2} \mathcal{B}(E_{CM}) dE_{CM}} \quad (14)$$

This expression can now be estimated by numerical integration based on the fitted parameters of $\mathcal{B}^*(E_{CM})$ (Eqs. 12 and 13). Even though the reproduction of the integral count by integration of the fitted function has in principle limited accuracy, rather accurate prediction of the relative error (Eq. 14) is achieved. The fit was performed on the deconvoluted histogram with the fixed parameters $E_0 = 3$ TeV and $\sigma = 13.7$ GeV, while b_{0-3} were varying freely. The resulting parameter values with the associated errors and the correlation matrix are shown below.

$$\begin{aligned} E_0 &= 3000 \\ \sigma &= 13.7 \\ b_0 &= (676.3 \pm 5.3) \times 10^3 \\ b_1 &= 539 \pm 23 \\ b_2 &= -0.66 \pm 0.15 \\ b_3 &= -0.446 \pm 0.010 \end{aligned} \quad (15)$$

$$\rho_{i,j} = \begin{pmatrix} 1 & 0.75 & 0.64 & 0.80 \\ 0.75 & 1 & 0.95 & 0.98 \\ 0.64 & 0.95 & 1 & 0.90 \\ 0.80 & 0.98 & 0.90 & 1 \end{pmatrix}$$

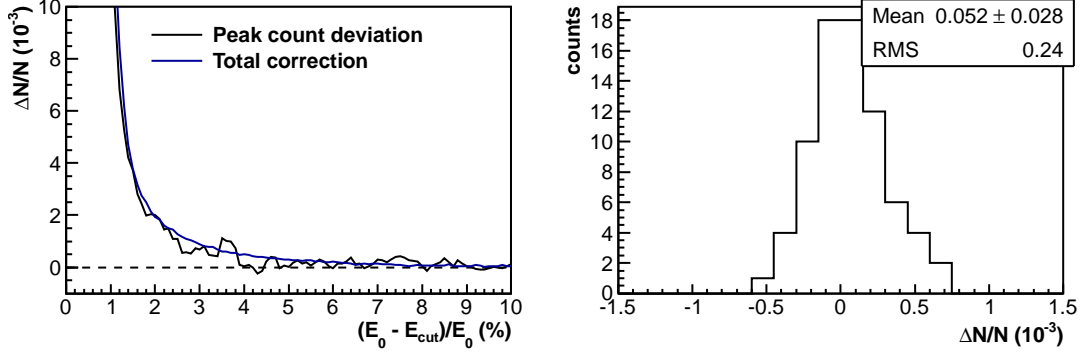


Figure 6: Left: relative deviation of the peak count induced by the LumiCal energy resolution in the reconstructed spectrum as a function of the peak region expressed as fraction of the nominal CM energy E_0 , compared to the predicted value based on the fitted spectrum. Right: histogram of the normalized residual deviations of the peak count after correction (see text), for E_{cut} more than 2.5% away from E_0 .

The relative deviation of the count in the reconstructed peak is shown in the left pane of Fig. 6 as a function of the relative distance of the energy cut to the peak energy in percent (black line). The predicted deviation according to Eq. 14 is also shown for comparison (blue line). There is an excellent agreement between the predicted and the simulated deviations. To take a safe distance from the peak, only points for which E_{cut} is more than 2.5% away from E_0 , corresponding to about 5σ of the fitted peak, will be considered in the following.

The fluctuations of the simulated deviation curve in Fig. 6 are of statistical nature. These fluctuations can be used as an external measure of the statistical uncertainty of the counting bias in the simulation. In the right pane in Fig. 6, the histogram of these fluctuations is shown, calculated as residual deviations after correction, for E_{cut} more than 2.5% away from E_0 . The RMS of the fluctuations corresponds to a relative statistical uncertainty of 0.24×10^{-3} with respect to the the peak count in the top 5%. The relative deviation in the top 5% estimated from Eq. 14 is -0.29×10^{-3} . The mean residual bias after correction is $(0.05 \pm 0.03) \times 10^{-5}$.

Similar procedure was applied to estimate the relative bias and the residual uncertainty in the tail region from 80% to 90% of E_0 . The RMS of the fluctuations is 0.79×10^{-3} , the uncorrected deviation is $+0.32 \times 10^{-3}$, and the residual deviation after correction is $(0.09 \pm 0.09) \times 10^{-3}$.

3.5 The Electromagnetic Deflection

To estimate the counting loss due to the EMD, the angular selection was applied once before and once after the deflection in the simulation, and the relative difference in the resulting number of events was calculated. The EMD counting loss above 95% of the nominal CM energy is $(-0.50 \pm 0.05) \times 10^{-3}$. In the tail from 80 to 90% of the nominal CM energy, the EMD counting loss is $(-1.08 \pm 0.08) \times 10^{-3}$.

4 Conclusions

A method of invariant counting of Bhabha events was presented. The number of Bhabha events within a given range of scattering angles in the collision frame, and in a given range of E_{CM} is reconstructed. The corresponding limits can be used for the cross-section integration in a straightforward way. In this way the luminosity expression (Eq. 1) is essentially insensitive to the beam-beam effects.

The residual systematic uncertainties of the Bhabha count with the presented methods were estimated by MC simulations. In addition, the systematic uncertainty due to the EMD-induced counting loss was estimated and found to be small. The residual relative errors in the top 5%, as well as in the tail from 80 to 90% of the nominal CM energy are listed in Tab. 2. Beam-beam effects in the luminosity measurement at CLIC can be corrected with a few permille precision.

The luminosity spectrum from 2.2 TeV to the maximum CM energy can be reconstructed from the deconvoluted Bhabha-event spectrum (Fig. 5).

Table 2: Relative residual error after correction of different systematic effects in luminosity measurement in the peak above 95% and the tail from 80 to 90% of the nominal CM energy.

#	Effect	Top 5% (10^{-3})	80 - 90% of E_0 (10^{-3})
1	Beamstrahlung-ISR angular loss	-0.1 ±0.4	-3.6 ±1.8
2	High β_{coll} ^a	-0.019±0.008	-2.7 ±0.1
3	ISR energy-loss	1.3 ±2.0	-2.3 ±3.9
4	Energy resolution	0.05 ±0.03	0.09±0.09
5	EMD counting loss (uncorrected)	-0.50 ±0.05	-1.08±0.08
	Total	1.4 ±2.0	4.4 ±4.3
	Total (corrected for #2) ^a	1.4 ±2.0	2.7 ±4.3

^a The bias under #2 is included in #1.

5 Acknowledgements

This work has been funded by the Ministry of science and education of the Republic of Serbia under the project Nr. OI 171012, "Physics and detector studies in HEP experiments". Additional travel grants from the CLIC Physics and Detectors study are gratefully acknowledged. The author wishes to thank the members of the Vinča HEP group and the FCAL collaboration for fruitful discussions. This work has been presented at the FCAL collaboration meeting in DESY Zeuthen, Germany, May 2012, and updated according to the ensuing discussion. Thanks to A. Sailer and D. Schlatter for a careful reading of the manuscript and many useful remarks.

References

- [1] S. Jadach. Theoretical error of luminosity cross section at LEP, 2003. ArXiv:hep-ph/0306083.
- [2] K. Yokoya and P. Chen. Beam-beam phenomena in linear colliders. In *Frontiers of Particle Beams: Intensity Limitations*, vol. 400 of *Lecture Notes in Physics*, pp. 415–445. Springer Verlag, 1991. US-CERN School on Particle Accelerators.
- [3] D. Schulte. *Study of Electromagnetic and Hadronic Background in the Interaction Region of the TESLA Collider*. Ph.D. thesis, Hamburg University, 1996.
- [4] D. Schulte, et al. Clic simulations from the start of the linac to the interaction point. In *Proceedings of EPAC 2002, Paris, France*, CERN-PS-2002-053-AE ; CLIC-Note-529. 2002.
- [5] C. Rimbault, P. Bambade, K. Mönig, and D. Schulte. Impact of beam-beam effects on precision luminosity measurements at the ILC. *Journal of Instrumentation*, vol. 2(09) p. P09001, 2007.
- [6] S. Jadach, W. Placzek, E. Richter-Was, B. Ward, and Z. Was. Upgrade of the monte carlo program BHLUMI for Bhabha scattering att low angles to version 4.04. *Computer Physics Communications*, vol. 102 p. 229, 1997.
- [7] I. Sadeh. *Luminosity Measurement at the International Linear Collider*. Master’s thesis, Tel Aviv University, 2008.
- [8] R. Schwartz. LumiCal performance in the CLIC environment - progress report. In *Proceedings of the 18th FCAL Workshop in Predeal, Romania*. 2011.
- [9] L. Linssen, A. Miyamoto, M. Stanitzki, and H. Weerts, eds. *Physics and Detectors at CLIC*. CERN-2012-003. CERN, 2012.
- [10] S. Lukić and I. Smiljanić. Correction of beam-beam effects in luminosity measurement at ILC, 2012. ArXiv:1211.6869.
- [11] J. Aguilar. Luminometer for the future international collider - simulation and beam test. In *Technology and Instrumentation in Particle Physics - TIPP 2011*. 2011. Preprint available at <http://arxiv.org/abs/1111.5199>.
- [12] T. Ohl. CIRCE version 1.0: Beam spectra for simulating linear collider physics. *Comput. Phys. Commun.*, vol. 101 p. 269, 1997.